Science Advances

AAAS

advances.sciencemag.org/cgi/content/full/4/5/eaar4298/DC1

Supplementary Materials for

Interface reconstruction with emerging charge ordering in hexagonal manganite

Shaobo Cheng, Changsong Xu, Shiqing Deng, Myung-Geun Han, Shanyong Bao, Jing Ma, Cewen Nan, Wenhui Duan, Laurent Bellaiche, Yimei Zhu, Jing Zhu

Published 18 May 2018, *Sci. Adv.* **4**, eaar4298 (2018)
DOI: 10.1126/sciadv.aar4298

This PDF file includes:

Supplementary Materials

1. EDS mapping at the $YMnO_3/Al_2O_3$ interface

Energy dispersive spectroscopy (EDS) experiments have been carried out to show the elemental distributions at the interface and results are presented in fig. S3. The experiments were conducted by FEI Themis 60-300 double spherical corrected TEM with SuperEDX attachment. Perhaps due to the interfacial effect, Mn ions close to the interface are more likely to be damaged within several minutes' EDS acquisition time. Atomic scale EDS result is hard to achieve due to the charging effect from the Al_2O_3 substrate. However, as shown in fig. S3B, two layers of Mn ions at the interface can still be well distinguished. The positions of Y and Mn atomic columns can be located in fig. S3D where Mn and Y signals are overlaid. Considering the structural relationship between $LuFeO_3$ and $LuFe_2O_4$, the $LuFe_2O_4$-like phase is realized at the $YMnO_3/Al_2O_3$ interface (*5*).

2. Distortions of oxygen bipyramids at the interfacial area

As shown in fig. S4A, the positions of oxygen can be clearly observed. By comparing the ABF images acquired from the interfacial area and the area far from the interface (named as the bulk area, shown in fig. S4B), it's easy to find that the oxygen bipyramids near the interface are distorted. In the bulk area, in the MnO plane, the oxygen and manganese are in the same atomic planes, while the oxygen shift downwards in the interfacial area, which is caused by the interfacial strain. Here, we define the distance between the oxygen plane and the Mn plane as *d*, whose value can be used to characterize the distortion of oxygen bipyramids. The positions of the atoms are located by Gaussian intensity fitting with MacTempasX commercial software and the *d* value is measured in each unit cell. The results can be found in fig. S4C. No shift of oxygen plane was observed in the bulk area and the *d* value is zero. *d* takes its largest value at the interface and decreases when moving away from the interface.

3. Identification of charge ordering by DFT calculations

Another distortion that the double layer experiences is the trimerization, which consists of the tilting of the MnO_5 bipyramid and the buckling of the adjacent Y layers (*8, 35*). Such effect is known in pure $YMnO_3$ films and has also been reported to lower the total energy of $LuFeO_3/LuFe_2O_4$ superlattices (*5*). In order to better understand the trimerization in each layer, we define, as shown in Fig. 3A of the manuscript, (i) the angle that MnO_5 tilts away from the *c*-axis in the sub-layers 1, sub-layers 2 and single Mn layers as θ_1, θ_2 and θ_3, respectively; and (ii) the vertical distance between Y ions moving up and down as Δ_1 in the Y layer 1 and as Δ_2 in the Y layer 2. It is numerically found, in the ground state of the studied superlattice combining a positive $\boldsymbol{P}_{sl}$ polarization along with ST1 and CO3 arrangements, that the averaged values of θ_1 and θ_2 are 2.76º and 1.23º, respectively, and Δ_1 and Δ_2 are 0.55 Å and 0.28 Å, respectively. Such data indicate a stronger trimerization in sub-layers 1 and their adjacent Y layers 1 than in sub-layers 2 and their adjacent Y layers 2. It is also found that θ_3 = 4.53º, which shows that trimerization in Mn single layers is much larger than that in the MnO double layers. One may also notice that the short Mn-O^{tp} bonds in sub-layers 1 (1.87 Å) render a smaller distance between Y layer 1 and sub-layer 1 than that between the Y layer 2 and sub-layer 2. Such small distance enables the hybridization between *d* orbitals of some Y ions (the ones that move down in the Y layer 1) and *p* orbitals of some O_1^{eq} ions in sub-layer 1 (*13, 36*) (see Fig. 3A and the black arrows marking displacements in Fig. 3C). The Y $d-O_1^{eq}$ p hybridization not only results in a stronger trimerization in sub-layer 1 but also leads to two types of MnO_5 bipyramids in sub-layer 2 (with a ratio of 1:2). The first type has longer Mn-O^{tp} bonds (2.00 and 2.42 Å in Fig. 3C) because of the Y $d-O_1^{eq}$ p hybridization,

while the other type has shorter Mn-O^{tp} bonds (1.97 and 2.17 Å in Fig. 3D) because of the lack of this *d* - *p* hybridization.

4. Polarization dependence of the charge ordering in MnO double layers

As shown in fig. S5, the polarization (displacements) of the $YMnO_3$ layer is gradually decreased (from ferroelectric $P6_3cm$ phase to paraelectric phase), while the MnO double layers are free to relax. The DFT calculation results show that, as long as the polarization of $YMnO_3$ layer is not reversed, the charge ordering of the MnO double layer will not be affected. On the other hand, once the polarization of $YMnO_3$ layer is reversed, the charge ordering of the MnO double layer will also be reversed.

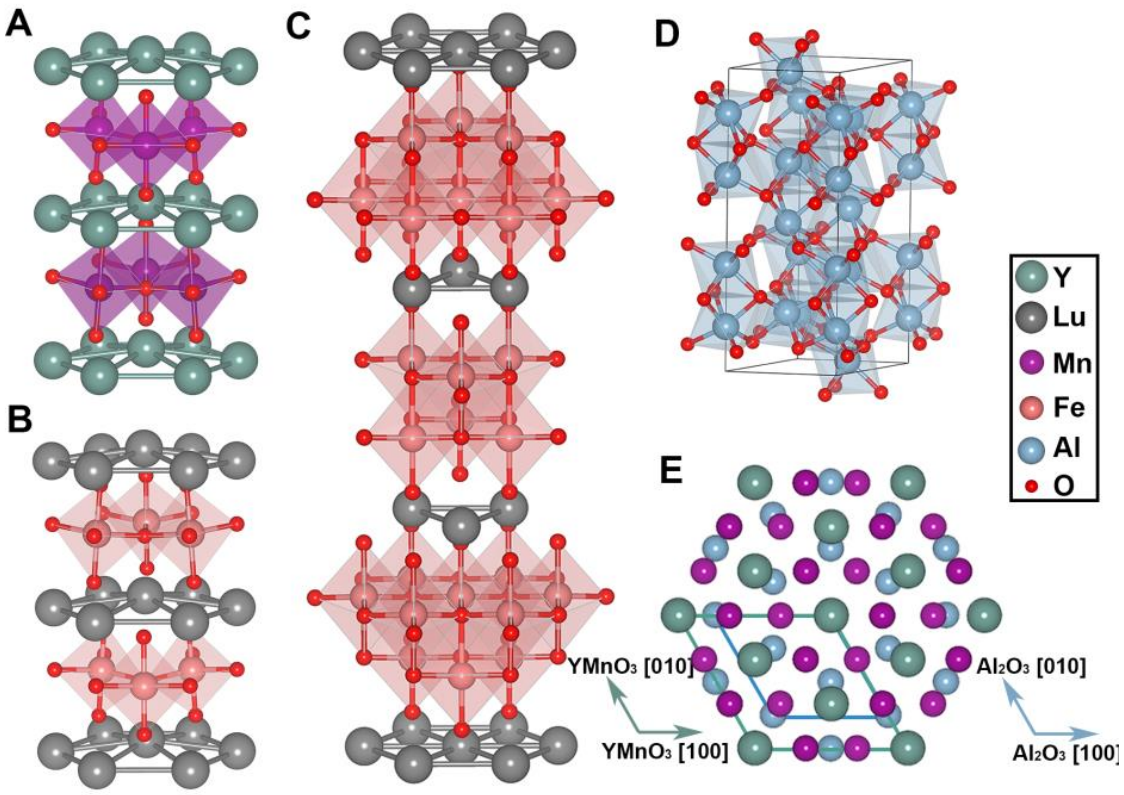

fig. S1. Schematic atomic models. (**A**) Downward polarized $YMnO_3$ hexagonal cell. Three nearby MnO_5 bipyramids tilt together and form trimerized configuration. (**B**) $LuFeO_3$ hexagonal cell having a similar atomic structure with $YMnO_3$. (**C**) Atomic structure of $LuFe_2O_4$. Three FeO double layers are stacked alternatively along the *c* direction. (**D**) α-Al_2O_3 unit cell. (**E**) Atomic arrangement of a $YMnO_3$ film grown on a *c*-Al_2O_3 substrate viewed along the [001] direction. The light blue and dark green parallelograms outline the unit cells of $YMnO_3$ and Al_2O_3, respectively.

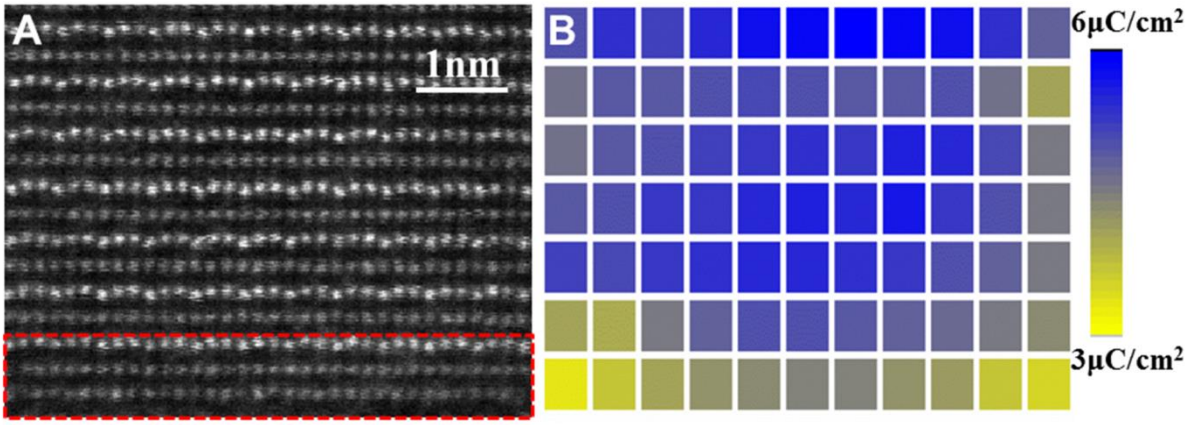

fig. S2. Quantitative evaluation of polarization in the film. (**A**) STEM image used for polarization mapping. Modified from Fig. 1D in the main text. (**B**) Calculated ferroelectric values from STEM image. Each box represents up-up-down polarization unit and the color represents the polarization value.

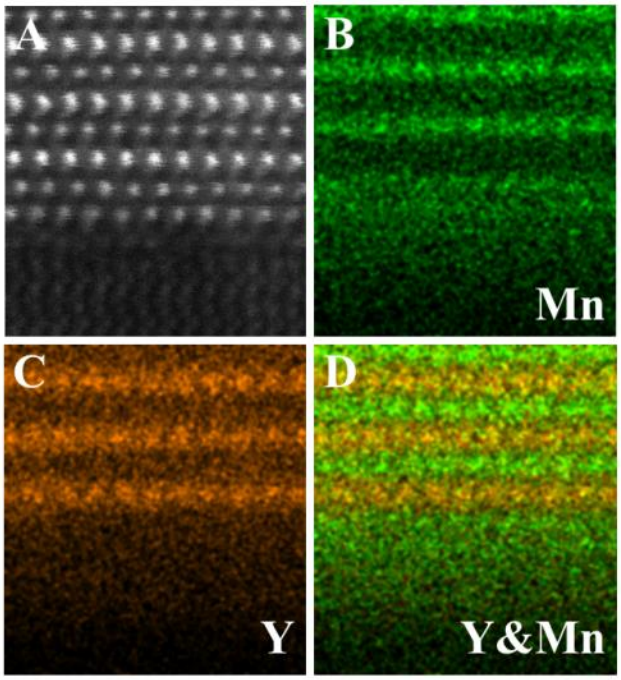

fig. S3. EDS mapping results for the interface. (**A**) HAADF image for the interested interfacial area. (**B**) Mn element mapping. (**C**) Y element mapping. (**D**) Combination of Y and Mn signals.

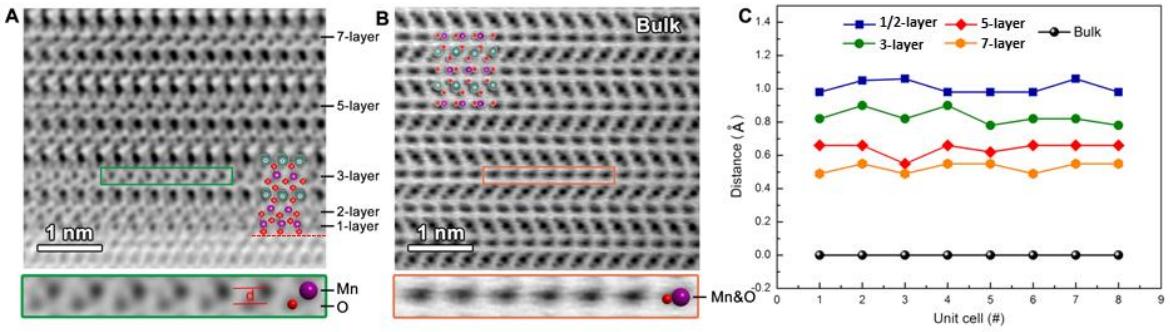

fig. S4. ABF images from the interfacial and the bulk areas. (**A**) ABF image showing the interface between $YMnO_3$ film and Al_2O_3 substrate viewing along the [210] zone axis. The atomic model of $YMnO_3$ is embedded. Y ions are in green, Mn in purple, O in red. The red horizontal line shows the interface. The sequential numbers for MnO layers are indicated. The area in green is magnified in the lower panel. (**B**) ABF image acquired from the area far from the interface (bulk area). The area in red is magnified. (**C**) Measurement for the distortion of oxygen bipyramids. The distortion is defined by the distance between the Mn plane and O plane as indicated by *d* in the lower panel in (A). No distortion in the bulk area and the distance is zero.

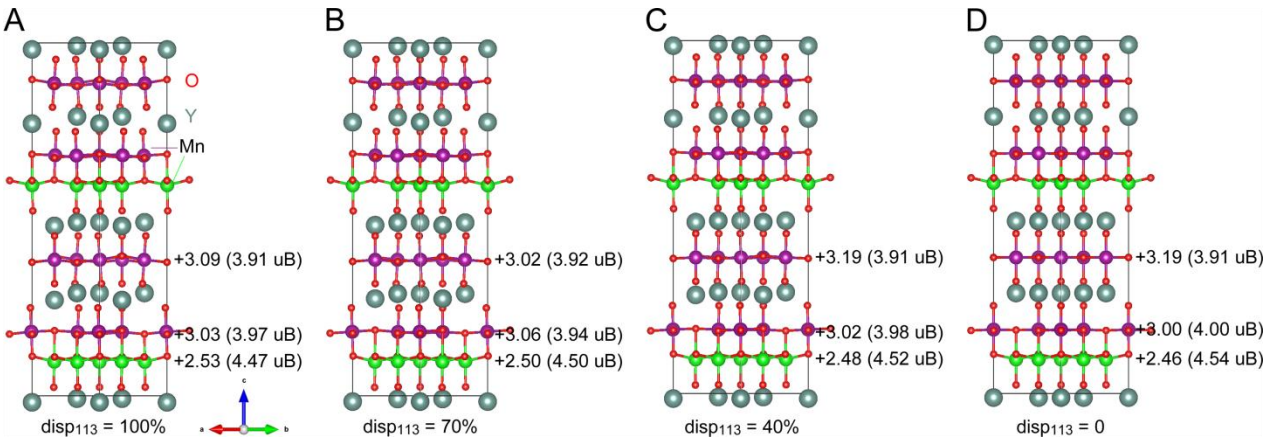

fig. S5. Calculated $YMnO_3$ polarization dependence of CO in MnO double layers. The polarization (displacements) of $YMnO_3$ layers are gradually decreased from (**A**) 100% (the fully relaxed structure) to (**B**) 70%, (**C**) 40% and (**D**) zero, while the structure and charge ordering of MnO double layer are optimized. The layer-averaged valence states, as well as the magnetic moments, are listed near each Mn-O layer in all panels.